3. NOISE/INTERFERENCE MODEL

3.1 Description of Model

Based on the case studies, a simple model of wideband HF noise/interference has been developed. The model is capable of describing the first-order statistics of all the aforementioned noise/interference data, and consists of three components:

- Gaussian noise
- Narrowband interferers (sine waves)
- Impulsive noise (filtered delta functions)

The presence of these three components is not unexpected, and is in accord with intuition. Within a bandwidth on the order of 1 MHz one expects contributions to the noise/interference from many independent sources, and hence, via the central limit theorem, a Gaussian component. On the other hand, one also expects many narrowband interferers, and if one or a few of these interferers are dominant, the central limit theorem no longer holds, so that these interferers must be included as a separate component of the model. Finally, it is well known that HF noise can be impulsive, due to atmospheric noise and other broadband manmade noise which is neither narrowband nor Gaussian, and must therefore be included as a third component of the model.

To make this precise, let x(t) denote the noise/interference signal at rf, and let the in-phase and quadrature components of the baseband signal be denoted by I(t) and Q(t), respectively. Then x(t) can be written as

$$x(t) = I(t)\cos\omega_0 t + Q(t)\sin\omega_0 t \qquad \textbf{(1)}$$

where ω_0 is the carrier frequency. The measured data correspond to I(t) and Q(t), which are the quantities we wish to model.

A sine wave of frequency ω can be written in the form of (1) by using the identity

$$\cos(\omega t + \phi) = \cos\omega_0 t\,\cos(\Delta\omega t + \phi) - \sin\omega_0 t\,\sin(\Delta t + \phi) \qquad \textbf{(2)}$$

where $\Delta\omega = \omega - \omega_0$ and φ is an arbitrary phase. The baseband components I and Q are the coefficients of $\cos\omega_0 t$ and $\sin\omega_0 t$, respectively.

Similarly, the baseband components of an impulse which arrives at time $t = t_0$ can be obtained by applying (2) to the Fourier integral representation of a delta function and transforming the variable of integration from ω to $\Delta\omega$:

$$\begin{aligned}\delta(t-t_0) &= \int_{-\infty}^{\infty} \cos\omega(t-t_0)\,d\omega \\ &= \cos\omega_0(t-t_0)\int_{-\infty}^{\infty}\cos\Delta\omega(t-t_0)\,d\Delta\omega \\ &= -\sin\omega_0(t-t_0)\int_{-\infty}^{\infty}\sin\Delta\omega(t-t_0)\,d\Delta\omega\end{aligned} \qquad \textbf{(3)}$$

Since we wish to model measured I and Q components which have been low-pass filtered, the upper and lower limits of the integrals in (3) should be replaced by $\pm 2\pi$ B, where B is the band-pass in Hz. The last integral in (3) vanishes because the $\sin\Delta\omega(t-t_0)$ is an odd function of $\Delta\omega$; evaluating the integral of $\cos\Delta\omega(t-t_0)$ and expanding $\cos\omega_0(t-t_0)$ enables one to express a filtered impulse $\delta_f(t-t_0)$ as

$$\delta_f(t-t_0) = \frac{\sin 2\pi B(t-t_0)}{t-t_0}\left(\cos\omega_0 t_0\,\cos\omega_0 t + \sin\omega_0 t_0\,\sin\omega_0 t\right) \qquad \textbf{(4)}$$

Again, the I and Q components correspond to the coefficients of $\cos\omega_0 t$ and $\sin\omega_0 t$, respectively. Combining results, the baseband components of the noise/interference model can be written as

$$I(t) = g_I(t) + \sum_{i=1}^{N_i} A_i\cos(\Delta\omega_i t + \phi_i + \sum_{j=1}^{N_j} B_j\frac{\sin 2\pi B(t-t_j)}{t-t_j}\cos\omega_0 t_j \qquad \textbf{(5)}$$

$$Q(t) = g_Q(t) - \sum_{i=1}^{N_i} A_i\sin(\Delta\omega_i t + \phi_i + \sum_{j=1}^{N_j} B_j\frac{\sin 2\pi B(t-t_j)}{t-t_j}\sin\omega_0 t_j \qquad \textbf{(6)}$$

where $g_I(t)$ and $g_Q(t)$ are independent, identically distributed zero-mean Gaussian processes, N_i is the number of narrowband interferers in the frequency band of interest, and N_j is the

number of impulses which occur during the time interval over which the noise/interference is being modeled.

Still to be specified are what fraction of the total noise/interference power is associated with each of the three components, how the narrowband interferers are distributed in amplitude, phase, and frequency, and how the noise impulses are distributed in amplitude and time. To do so, the results of the various case studies discussed above were examined.

It was concluded that the frequency and phase distributions of the narrowband interferers are uniform. As discussed in Section 2.3.1, the amplitude distribution of the narrowband interferers can be obtained from the cdf of the power envelope in the frequency domain. This has been shown by Lemmon (1989) to be well described by a combination of a Gaussian process and an impulsive process defined by a model developed by Hall (1966). It may seem inappropriate to use a model of impulsive phenomena to describe narrowband interferers; however, narrowband interferers are impulsive in the frequency domain, and it is the amplitude distribution of these frequency domain impulses that must be described. Thus, it was concluded that the pdf for the amplitudes A_i can be modeled by the amplitude pdf of the Hall model:

$$p(A) = \frac{(\theta - 1)\gamma^{\theta-1} A}{\left(A^2 + \gamma^2\right)^{(\theta+1)/2}} \qquad \textbf{(7)}$$

The model has two free parameters, θ and γ. Roughly speaking, the value of θ determines the slope of the power cdf at high power levels, where the cdf is approximately linear (on log-log scales), and the value of γ determines the overall power scale.

A possible objection to modeling the amplitude distribution as a pure "Hall" process is that although the power cdf in the frequency domain is well described by a combination of Gaussian and Hall processes, and although the noise/interference in the time domain is assumed to consist of a combination of a Gaussian process and narrowband interferers (in the absence of impulsive noise), it has not been shown that the Gaussian process in the time domain corresponds to a Gaussian process in the frequency domain. Thus, it has not been shown that the narrowband interferers in the time domain correspond to a Hall process in the frequency domain.

That this is indeed the case, however, can be seen by the following argument. The Rice representation for zero-mean Gaussian noise (Rice, 1944 and 1945) in a time interval of length T and in a frequency band from -B to B can be written as

$$g(t) = \sum_{n=1}^{BT_i} \left(a_n \cos \frac{2\pi nt}{T} + b_n \sin \frac{2\pi nt}{T} \right) \qquad \textbf{(8)}$$

where the Fourier coefficients a_n and b_n are independent random variables which are Gaussian distributed with zero means. Here the distribution of a given coefficient (fixed value of n) refers to the distribution of values of that coefficient obtained from an ensemble of noise records. Note that a_n and b_n correspond to the real and imaginary parts, respectively, of the Fourier transform of g(t).

Now consider a single noise record and the distribution p(a) of the set of values of a_n for n= 1,2,...,BT. We wish to determine under what circumstances p(a) is a Gaussian. Note that p(a) can be viewed as the probability that a given a_n is.sampled, times the pdf of a_n for that value of n, summed over n. The probability that a given a_n is sampled is 1/BT. Thus, p(a) can be written as

$$p(a) = \frac{1}{\sqrt{2\pi}BT} \sum_{n=1}^{BT} \frac{e^{-a^2/\sigma^2(a_n)}}{\sigma(a_n)} \qquad \textbf{(9)}$$

where $\sigma(a_n)$ is the standard deviation of the pdf of a_n. Since Gaussians with different standard deviations are linearly independent, and since (9) is a sum of Gaussians, it is easy to see that p(a) is a Gaussian if and only if the $\sigma(a_n)$ are equal to one another for all n. A similar argument holds for the b_n. Therefore, the Fourier transform of a (real) Gaussian process g(t) is a (complex) Gaussian process in the frequency domain if and only if g(t) is white Gaussian noise, that is, Gaussian noise whose spectral properties (i.e., the a_n and b_n) are independent of frequency.

The argument can be generalized to include the case of a complex Gaussian process g(t). Thus, the Fourier transform of a complex Gaussian process is a complex Gaussian process in the frequency domain if and only if g(t) is white. Although we have no proof that

the Gaussian component of actual noise/interference is white, the power spectra shown in the previous examples strongly suggest this to be the case.

It is of interest to see that modeling the noise/interference as a combination of Gaussian and "Hall" processes in the frequency domain leads to a nonuniform phase distribution in the. frequency domain, even though the Gaussian and Hall processes individually have uniform phase distributions. Let G(ω) and H(ω) denote the in-phase components. of a complex Gaussian and a complex "Hall" process, respectively, in the frequency domain, and let their corresponding quadrature components be denoted by $\widetilde{G}$ (ω) and $\widetilde{H}$(ω). Then the joint pdf $p_{x,\tilde{x}}(x,\tilde{x})$ for the combined process X = G + H, $\widetilde{X} = \widetilde{G} + \widetilde{H}$ can be written as a double convolution integral:

$$p_{x,\tilde{x}}(x,\tilde{x}) = \int_{-\infty}^{\infty}\int_{-\infty}^{\infty} p_{H,\tilde{H}}\left(x-z,\tilde{x}-\tilde{z}\right)p_{G,\tilde{G}}\left(z,\tilde{z}\right)dzd\tilde{z} \qquad \textbf{(10)}$$

where $p_{H,\tilde{H}}$ and $p_{G,\tilde{G}}$ denote the joint pdfs for the Hall and Gaussian processes, respectively. An expression for $p_{H,\tilde{H}}$ has been derived by Hall (1966):

$$p_{H,\tilde{H}}(x,\tilde{x}) \propto \frac{1}{\left(x^2+\tilde{x}^2+\gamma^2\right)^{(\theta+1)/2}} \qquad \textbf{(11)}$$

Since G and $\widetilde{G}$ are independent, identically distributed Gaussian processes, $p_{G,\tilde{G}}$ can be written as

$$p_{G,\tilde{G}}(x,\tilde{x}) \propto e^{-\left(x^2+\tilde{x}^2\right)/2\sigma^2} \qquad \textbf{(12)}$$

Substituting (11) and (12) into (10) gives

$$p_{x,\tilde{x}}(x,\tilde{x}) \propto \int_{-\infty}^{\infty}\int_{-\infty}^{\infty} \frac{e^{-\left(z^2+\tilde{z}^2\right)/2\sigma^2}}{\left[\left(x-z\right)^2+\left(\tilde{x}-\tilde{z}\right)^2+\gamma^2\right]^{(\theta+1)/2}}dzd\tilde{z} \qquad \textbf{(13)}$$

Making a transformation of variables from $(x,\tilde{x})$ to (V,φ) via

$$x^2 + \tilde{x}^2 = V^2 \tag{14}$$

$$x^2 + \tilde{x}^2 = V^2 \tag{15}$$

$$x^2 + \tilde{x}^2 = V^2 \tag{16}$$

results in the joint pdf $p_{v,\varphi}$ in amplitude V and phase φ for the combined process:

$$p_{v,\phi} = v p_{x,\tilde{x}} \propto \int_{-\infty}^{\infty}\int_{-\infty}^{\infty} v \frac{e^{-\left(z^2+\tilde{z}^2\right)/2\sigma^2}}{\left[V^2 - 2zV\cos\phi - 2\tilde{z}V\sin\phi + z^2 + \tilde{z}^2 + \gamma^2\right]^{(\theta+1)/2}} dz d\tilde{z} \tag{17}$$

Finally, the phase distribution p_φ is obtained from the joint distribution $p_{v,\varphi}$ by integrating over V,

$$p_\phi = \int_0^{\infty} p_{v,\phi} dV \tag{18}$$

so that

$$p_\phi \propto \int_0^{\infty} dV \int_{-\infty}^{\infty} dz \int_{-\infty}^{\infty} d\tilde{z} \frac{V e^{-\left(z^2+\tilde{z}^2\right)/2\sigma^2}}{\left[V^2 - 2zV\cos\phi - 2\tilde{z}V\sin\phi + z^2 + \tilde{z}^2 + \gamma^2\right]^{(\theta+1)/2}} \tag{19}$$

Although no attempt has been made to evaluate the triple integral in (19), it is clear that p_φ is not uniform, but is φ-dependent, and has a period of 2π.

Turning now to the impulsive noise, it was concluded from examination of the power cdf's in the time domain that the amplitude distribution of the impulses can also be described by that of the Hall model for amplitudes B_j which are less than some maximum value B_{max}. At larger values of amplitude, the distribution appears to be cut off (relative to that of the Hall model). Whether this is due to some intrinsic property of the noise pulses or is due to the limited dynamic range of the receiving and data acquisition systems remains unclear at this time; the resolution of this question will require additional data

obtained with a system that has greater dynamic range. In any case, based upon these observations, it is proposed that the amplitude distribution p(B) of the impulses in the time domain be modeled by that of a cutoff Hall model:

$$p(B) = \left\{ 0 \frac{1-\theta}{\left(B_{\max}^2 + \gamma^2\right)^{(1-\theta)/2} - \gamma^{2(1-\theta)/2}} \cdot \frac{B}{B>B_{\max}} \left(B^2 + \gamma^2\right)^{(\theta+1)/2}, 0 \le B \le B_{\max} \right\} \qquad \textbf{(20)}$$

The expression in the first line of (20) differs from that in (7) because cutting off the distribution results in a different normalization constant.

As discussed in Section 2.3.5, in the one noise record which clearly exhibits impulsive noise, the noise impulses do not occur randomly in time, but tend to occur in a quasi-periodic fashion. However, quantitatively modeling the arrival time distribution requires investigation of the noise pulse spacing distribution, and this, as well as investigation of the other higher-order statistics, is beyond the scope of the present work, and will not be further discussed in this report. For the present purposes of modeling the first-order statistics, the pulse arrival distribution will therefore be assumed to be uniform.

3.2 Comparisons of Model with Measurements

To demonstrate the usefulness of the model for simulation purposes, noise/interference has been simulated, analyzed, and compared to the corresponding analyses of measured data for two particular noise/interference environments: the case study discussed in Section 2.3.1, which is typical of the data examined in the 42 noise records, and the case study discussed in Section 2.3.5, which exhibits impulsive noise, in addition to the Gaussian and narrowband components. The purpose of these comparisons is not to exhibit simulated results which are identical to the corresponding measured results, but rather to demonstrate that the model generates noise/interference with the same statistical characteristics as the measured data.

In the first case, the simulated noise/interference consists of a combination of Gaussian noise and 40 sine waves. Each sample of the Gaussian noise was generated by summing 12 random variables, uniformly distributed between -0.5 and 0.5. Since the mean and variance of each of the random variables are 0 and 1/12, respectively, the mean and variance of the composite process are 0 and 1, respectively. The central limit theorem

implies that the composite process is (approximately) Gaussian, as discussed, for example, by Mihram (1972). Moreover, because each sample was generated independently of the others, the autocorrelation function of the process is impulsive; thus, its Fourier transform (the power spectrum) is flat, and the noise is therefore white.

The model specifies that the amplitudes A_i of the sine waves are distributed according to (7). A set of amplitudes so distributed can be generated by integrating (7) to obtain the cumulative probability P(A),

$$P(A) = 1 - \frac{\gamma^{\theta-1}}{\left(A^2 + \gamma^2\right)^{(\theta-1)/2}} \tag{21}$$

inverting the result to obtain A(P),

$$A(P) = \gamma\left[\frac{1}{(1-P)^{2/(\theta-1)}} - 1\right]^{1/2} \tag{22}$$

and viewing the cumulative probability P as a random variable uniformly distributed between 0 and 1. Thus, random values of P, uniformly distributed between 0 and 1, were generated and substituted into (22) to obtain values of A_i. The values of the parameters γ and θ were chosen to be $\gamma = 0.3$ and $\theta = 2.0$.

The phases φ_i of the sine waves are uniformly distributed between 0 and 2π, and the baseband frequencies $\Delta\omega_i$ are uniformly distributed between -400 kHz and +400 kHz.

Plots of the I-channel data, both measured and simulated, over an interval of 4 ms, are shown in Figure 39. Although the measured and simulated data are qualitatively similar, the simulated data appears to have more high frequency noise than the measured data. However, this is due to the fact that the frequency of the dominant narrowband interferer in the simulated data happens to be higher than that in the measured data in this particular case. Because the frequencies and amplitudes of the narrowband interferers are treated as random variables in the simulation, it is unlikely that the measured and simulated data will exhibit identical sets of narrowband interferers. Nevertheless, the statistical properties of the measured and simulated data are quite similar, as can be seen by comparing the measured and simulated pdf's of the I-channel data, the power envelope, and the phase, which are shown in Figures 40, 41, and 42, respectively.

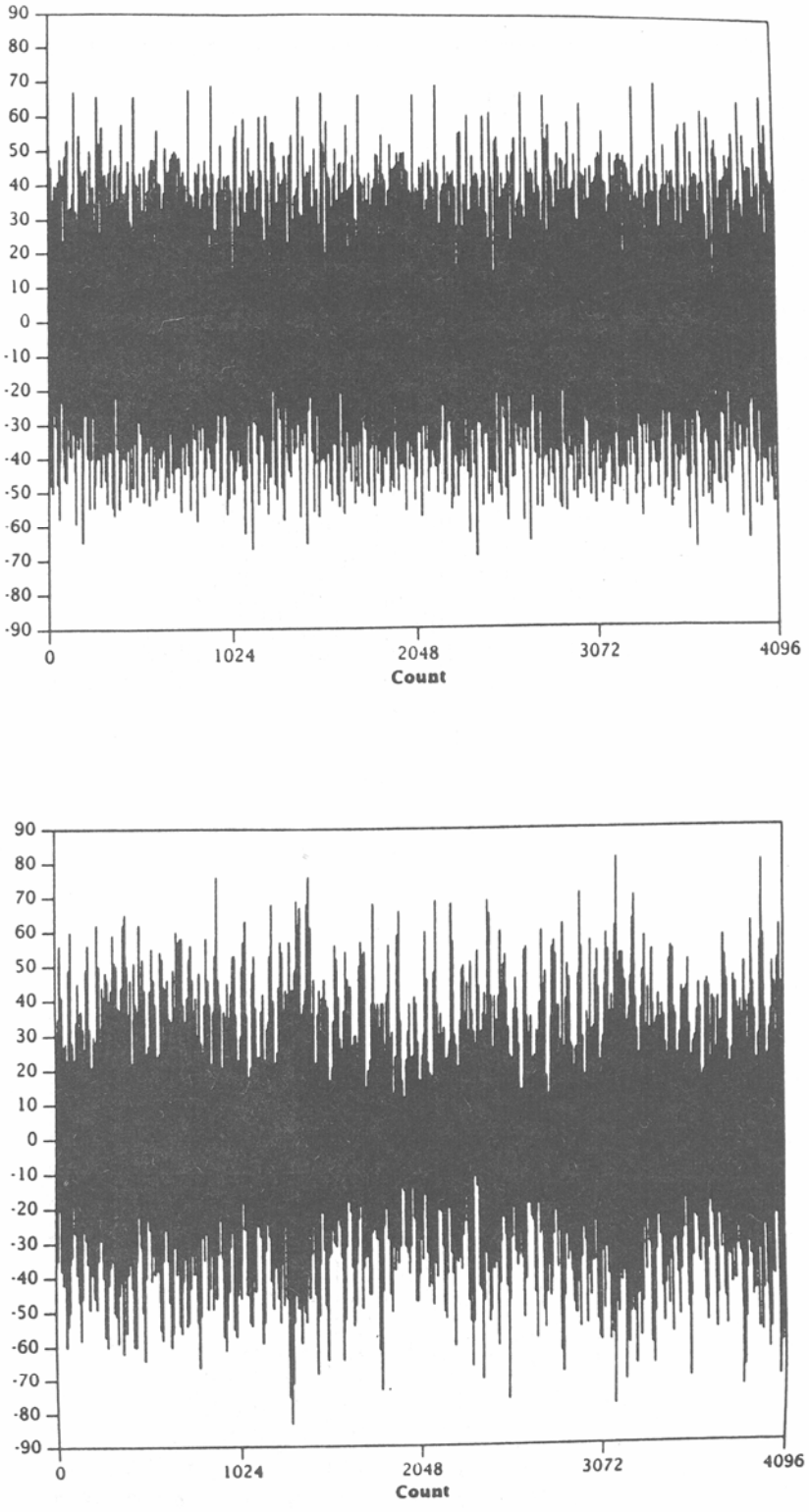

Figure 39. Comparison of (a) simulated and (b) measured (case study 1) noise/interference in the I-channel data.

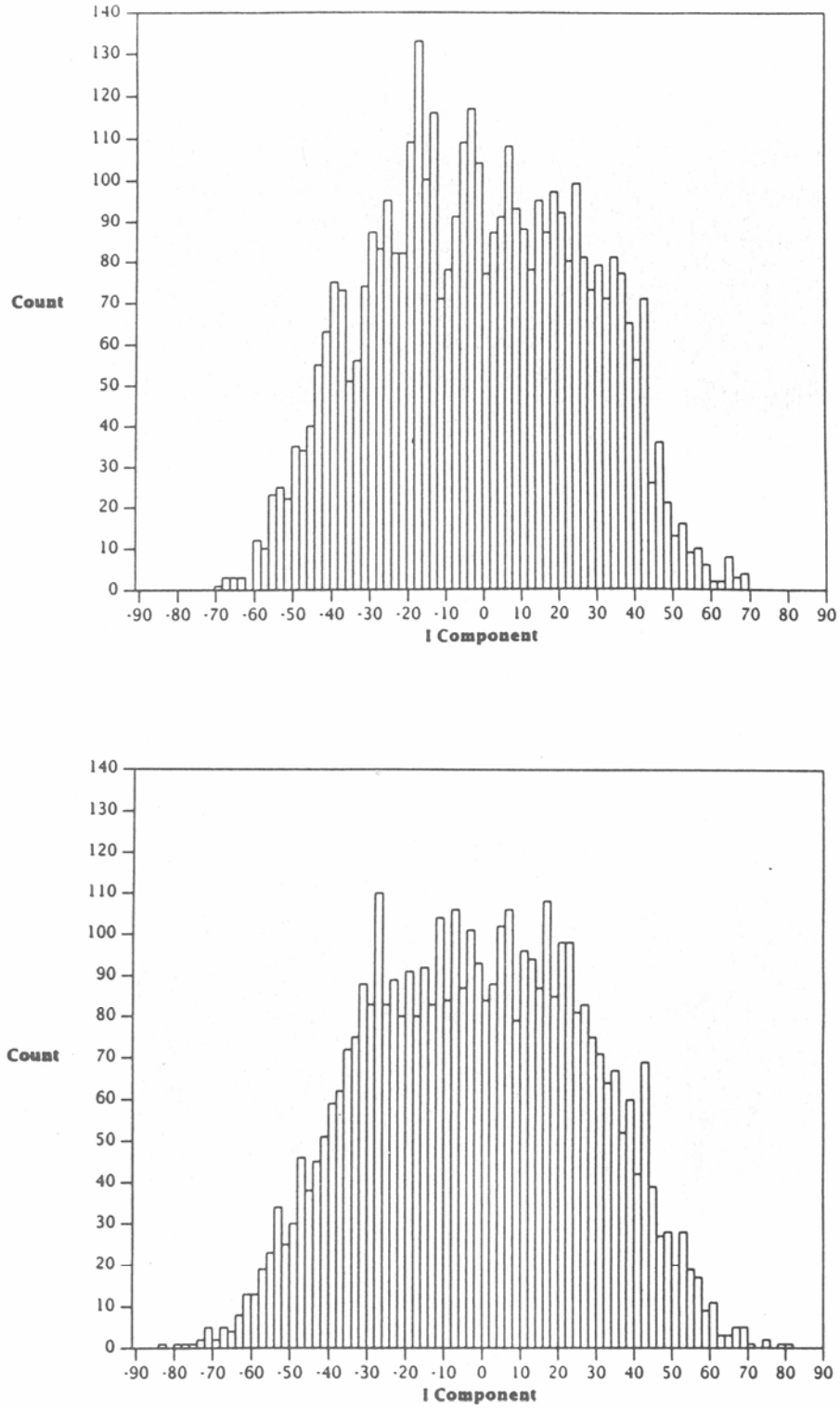

Figure 40. Comparison of (a) simulated and (b) measured (case study 1) probability density functions of the I-channel data.

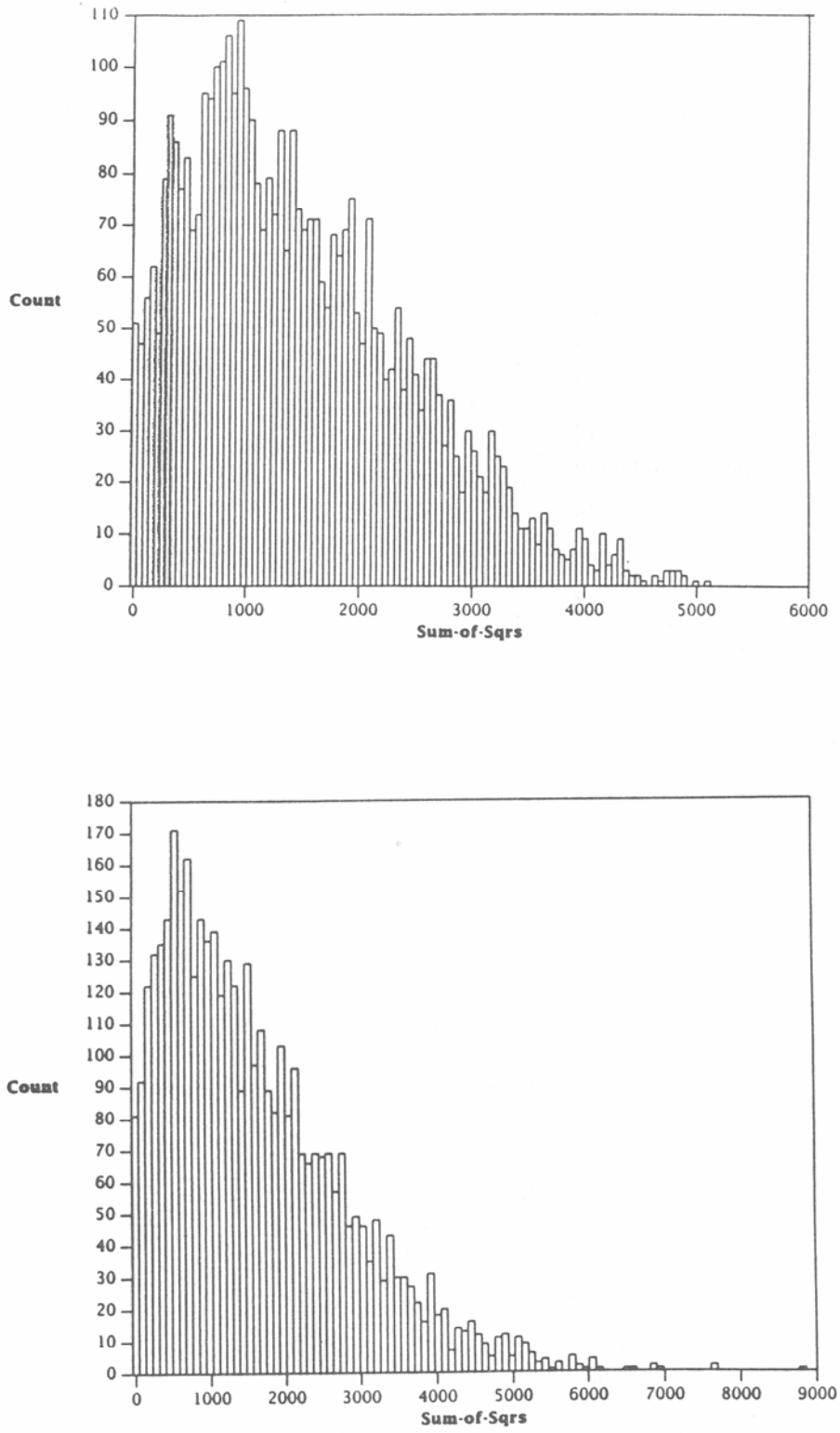

Figure 41. Comparison of (a) simulated and (b) measured (case study 1) probability density functions of the power envelope in the time domain.

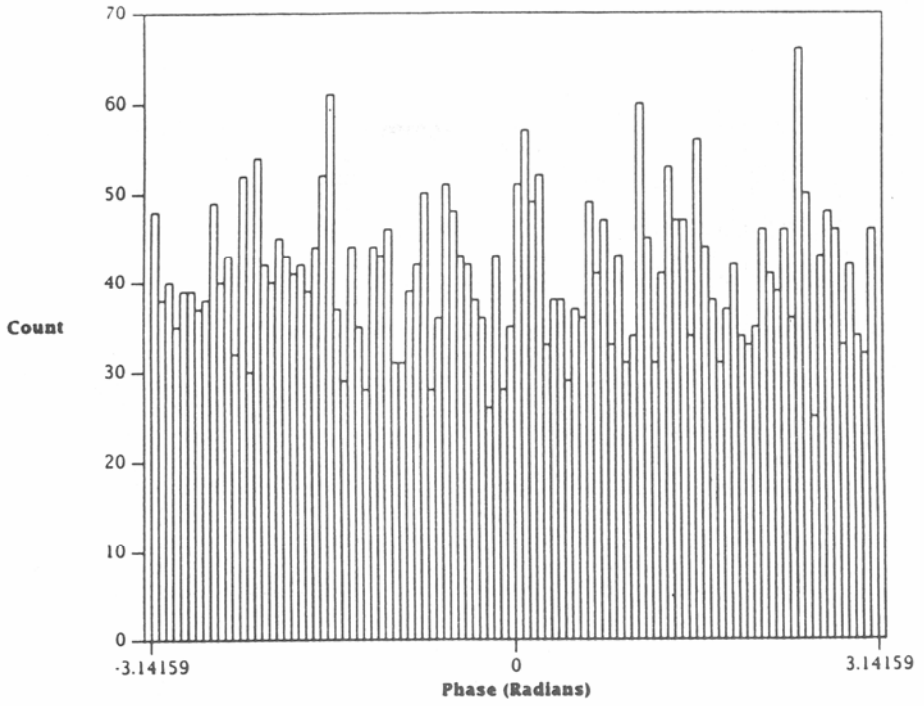

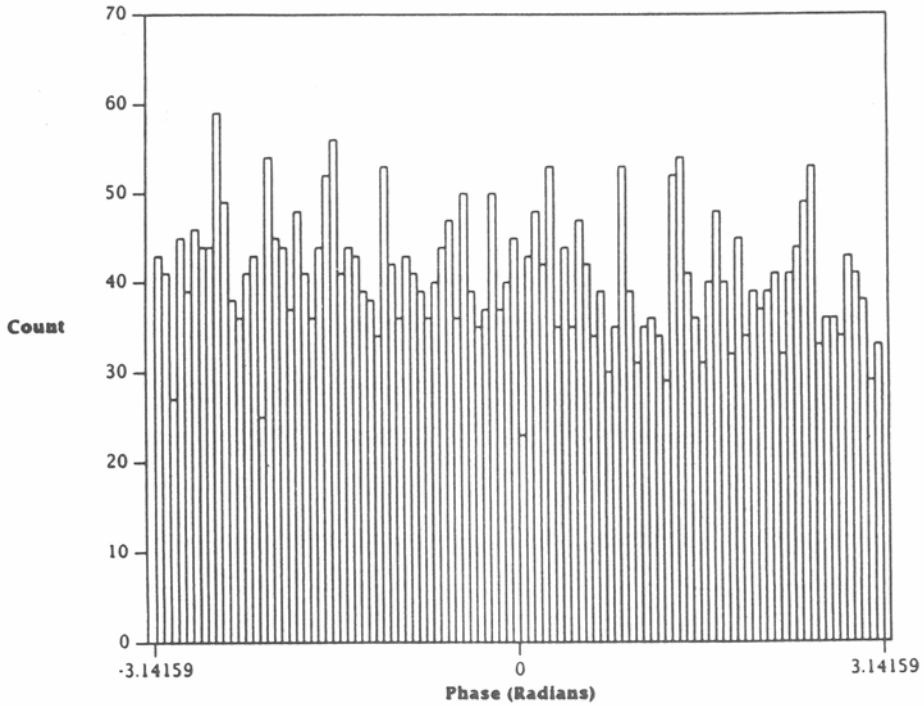

Figure 42. Comparison of (a) simulated and (b) measured (case study 1) probability density functions of the phase in the time domain.

65

The level crossing distributions of the voltage envelope are shown in Figure 43. Again, the measured and simulated distributions are qualitatively similar, although the scale of the simulated distribution is nearly three times larger than that of the measured distribution. This is to be expected if the frequency of the dominant narrowband interferer in the simulated data is several times greater than that in the measured data.

That this is indeed the case can be seen by comparing the measured and simulated power spectra, shown in Figure 44. Whereas the frequency of the dominant interferer in the simulated data is approximately 350 kHz, the frequencies of the dominant interferers in the measured data tend to cluster around -125 kHz. Also note that the spectral lines corresponding to the dominant interferers have a finite width, even though they have been modeled by zero bandwidth sine and cosine waves. The reason is because the power spectrum is the square of the Fourier transform of a noise record of finite length (4 ms) and the Fourier transform of a complex exponential $e^{i\Delta\omega t}$ of finite time duration is a linear combination of a filtered impulse and its Hilbert transform:

$$\int_0^T e^{-i\Delta\omega t} e^{i\omega t}\, dt = \frac{1}{\omega - \Delta\omega}\left\{\sin\left(\omega - \Delta\omega\right)T - i\left[\cos\left(\omega - \Delta\omega\right)T - 1\right]\right\} \qquad \textbf{(23)}$$

Thus, the structure of the spectral lines in the power spectrum corresponds to the logarithm of the envelope $1/(\omega\text{-}\Delta\omega)^2$.

The cdf's of the power envelope in the frequency domain and the pdf's of the phase in the frequency domain are shown in Figures 45 and 46, respectively. The similarity of the measured and simulated power envelope cdf's is to be expected, because the amplitude distribution of the sine waves in the simulation was chosen to reproduce the measured distribution. The simulated phase distribution is nonuniform, as expected based on the discussion in Section 3.1, and also is qualitatively similar to the measured distribution, although shifted in phase. However, a relative phase shift in the frequency domain corresponds to a relative time shift of the noise record, which is of no physical significance.

The noise/interference discussed in Section 2.3.5 was simulated by combining Gaussian noise, 40 sine waves, and 50 impulses. The Gaussian noise and sine waves were

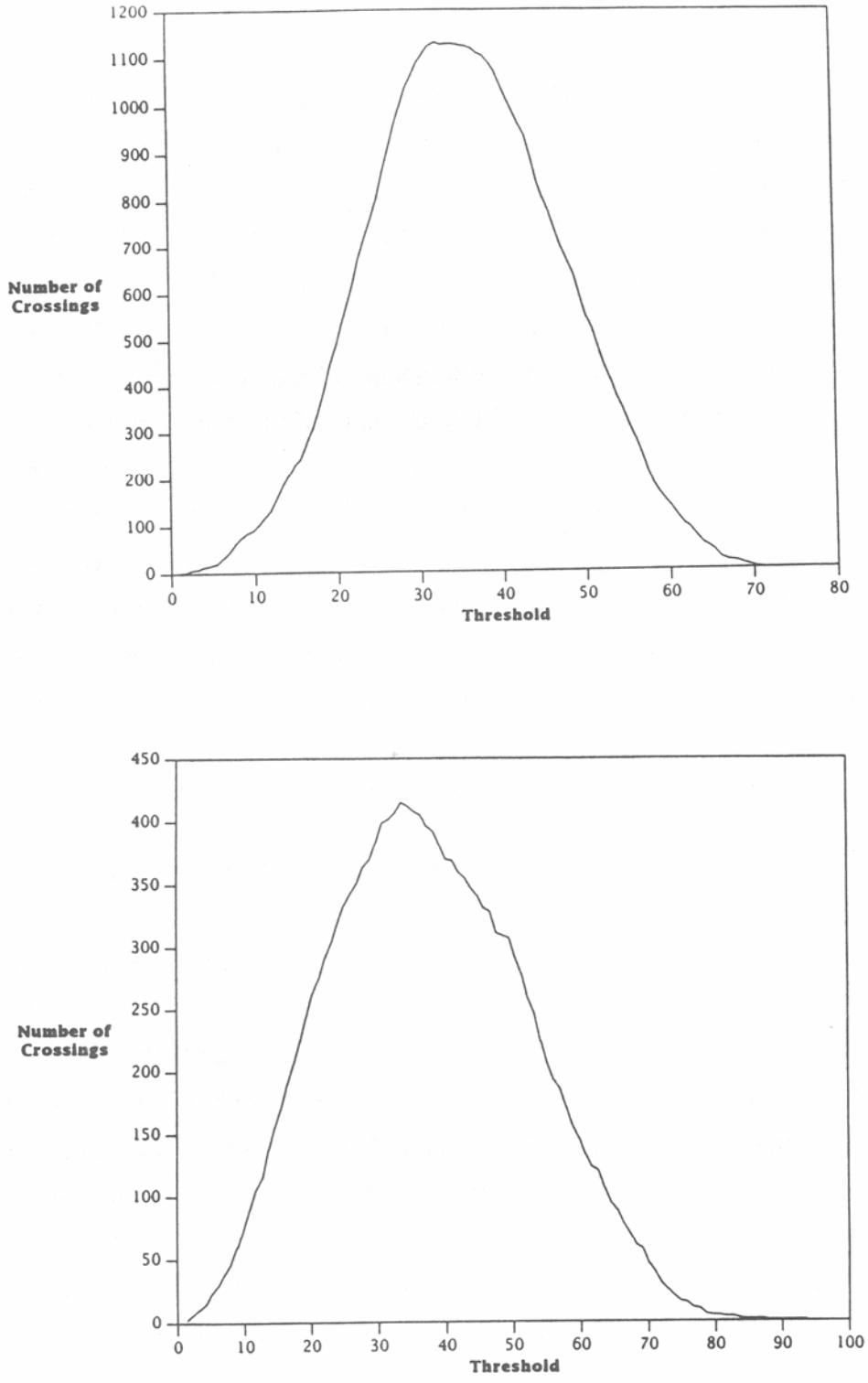

Figure 43. Comparison of (a) simulated and (b) measured (case study 1) level crossing distributions of the voltage envelope.

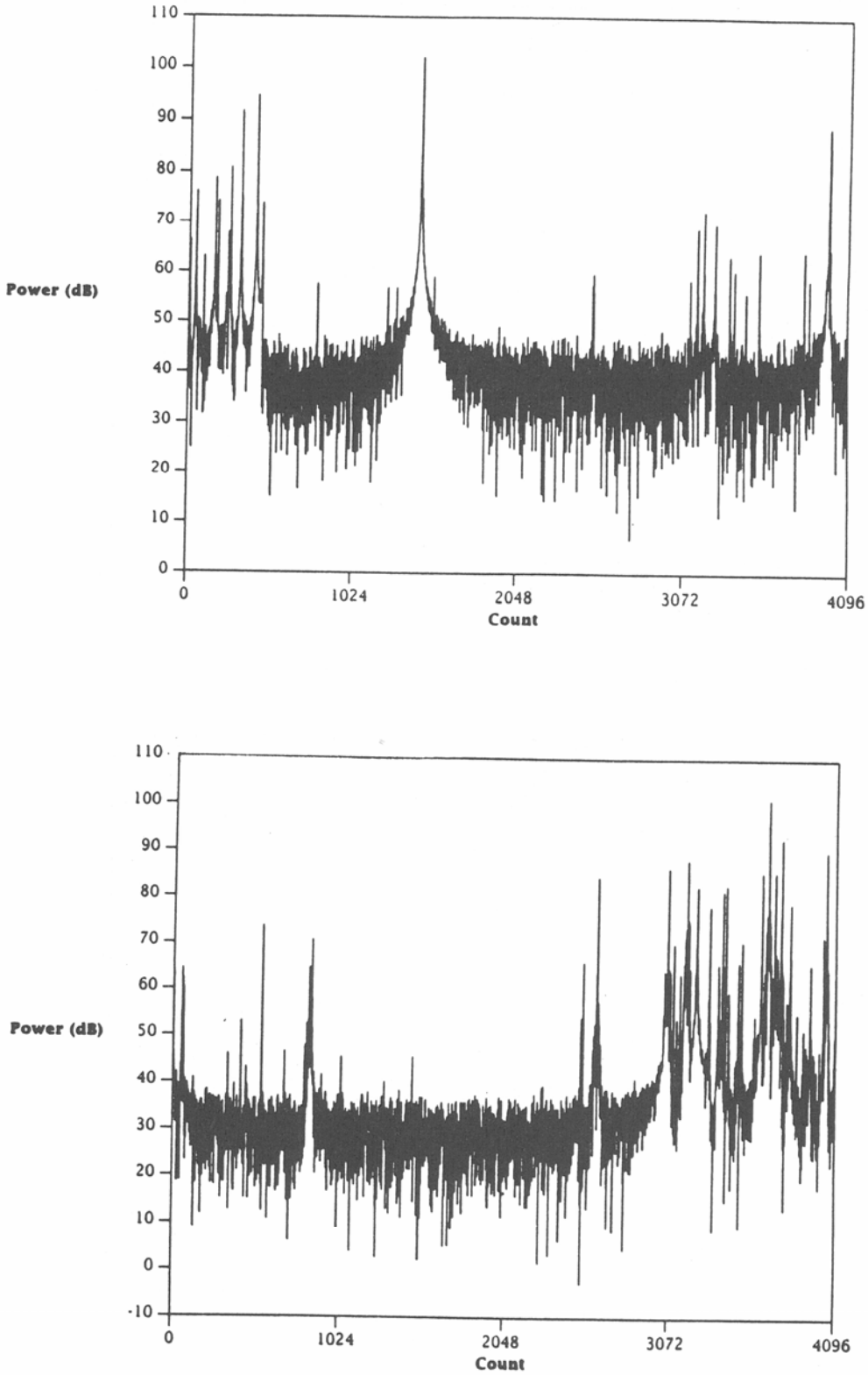

Figure 44. Comparison of (a) simulated and (b) measured (case study 1) power spectra.

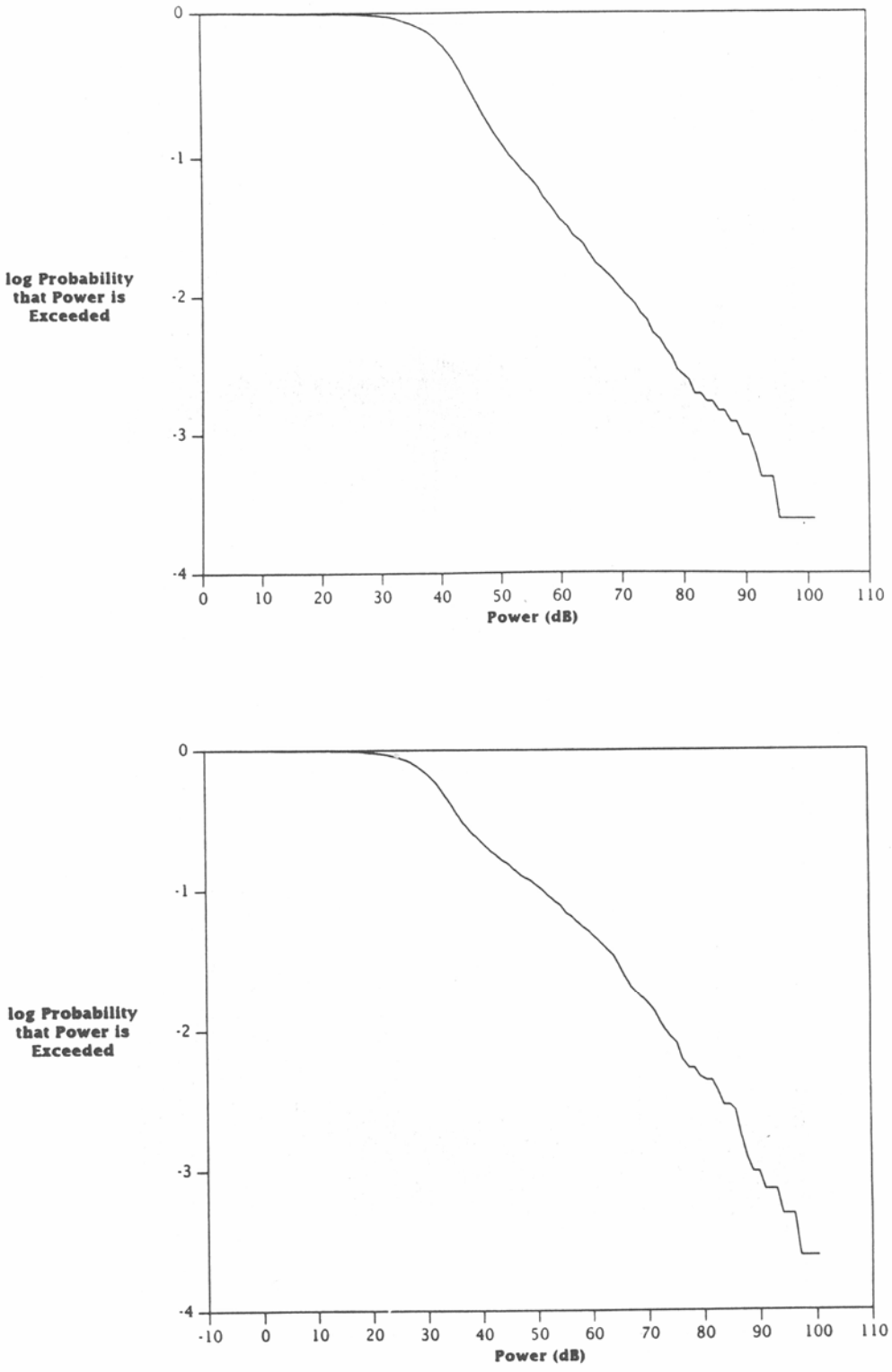

Figure 45. Comparison of (a) simulated and (b) measured (case study 1) cumulative distribution functions of the power envelope in the frequency domain.

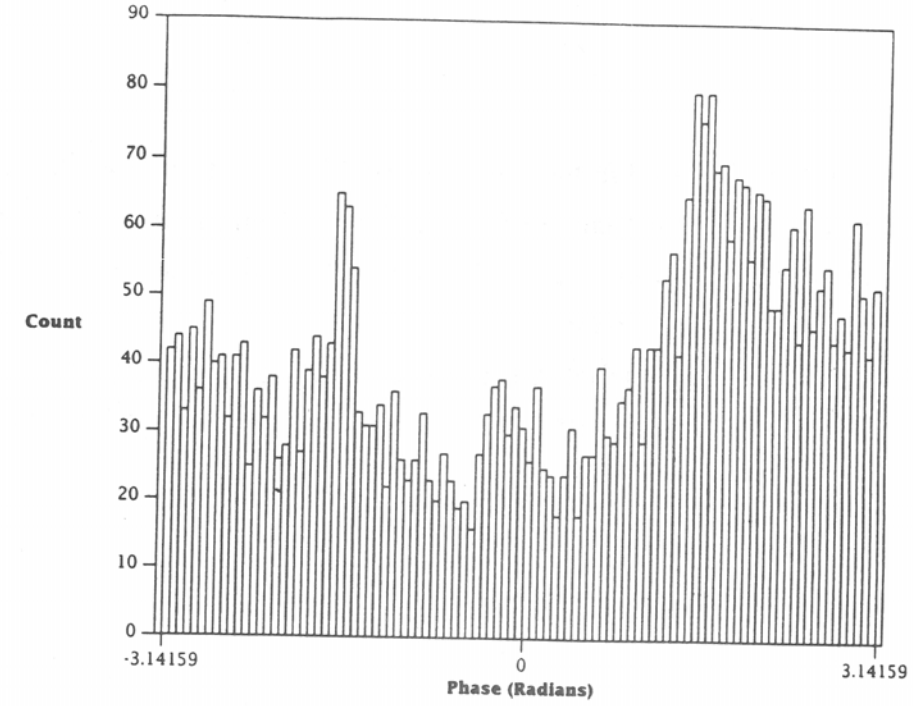

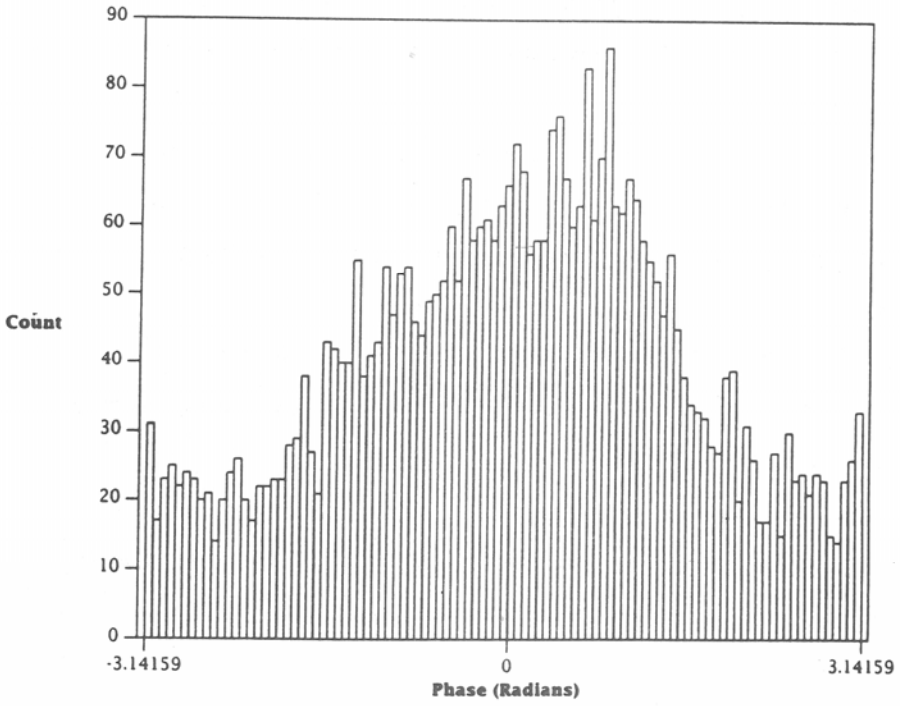

Figure 46. Comparison of (a) simulated and (b) measured (case study 1) probability density functions of the phase in the frequency domain.

generated by the techniques discussed in the previous example, except that the Gaussian noise samples were multiplied by a factor of 0.12, so that $g_I(t)$ and $g_Q(t)$ each have a variance σ^2=0.0144, and the parameters γ and θ in the amplitude distribution of the sine waves were chosen to be $\gamma = 0.2$ and $\theta = 2.0$.

The amplitudes B_j of the impulses are distributed according to (20) and were generated by a technique analogous to that used to generate the A_i. Integrating (20) to obtain the cumulative distribution P(B),

$$P(B) = \frac{\left(B^2 + \gamma^2\right)^{(1-\theta)/2} - \gamma^{2(1-\theta)/2}}{\left(B_{\max}^2 + \gamma^2\right)^{(1-\theta)/2} - \gamma^{2(1-\theta)/2}} \tag{24}$$

and inverting to obtain B(P),

$$B(P) = \gamma\left\{\left[P\left[\left(\frac{B_{\max}^2}{\gamma^2}+1\right)^{(1-\theta)/2} - 1\right]+1\right]^{2/(1-\theta)} - 1\right\}^{1/2} \tag{25}$$

values of B_j were obtained by generating random values of P**,** uniformly distributed between 0 and 1, and substituting into (25). The parameters were chosen to be $B_{max}=2\text{x}10^{-5}$, $\gamma = 1.0\text{x}10^{-8}$, and $\theta = 1.2$.

The arrival times t_j of the impulses are uniformly distributed between 0 and 4 ms.

Plots of the I-channel data and pdf's of these data are shown in Figures 47 and 48, respectively. The presence of impulses in the raw data results in the long tails in the pdf's, which otherwise are typical of those of previous case studies.

The pdf's of the power envelope, which are shown in Figure 49, also exhibit long tails, which are more readily apparent in the cdf of the power envelope plotted on log-log scales, as shown in Figure 50.

The pdf's of the phase in the time domain are shown in Figure 51. As discussed above, the spikes in the measured distribution are an artifact of the A/D conversion, and are intentionally not being simulated.

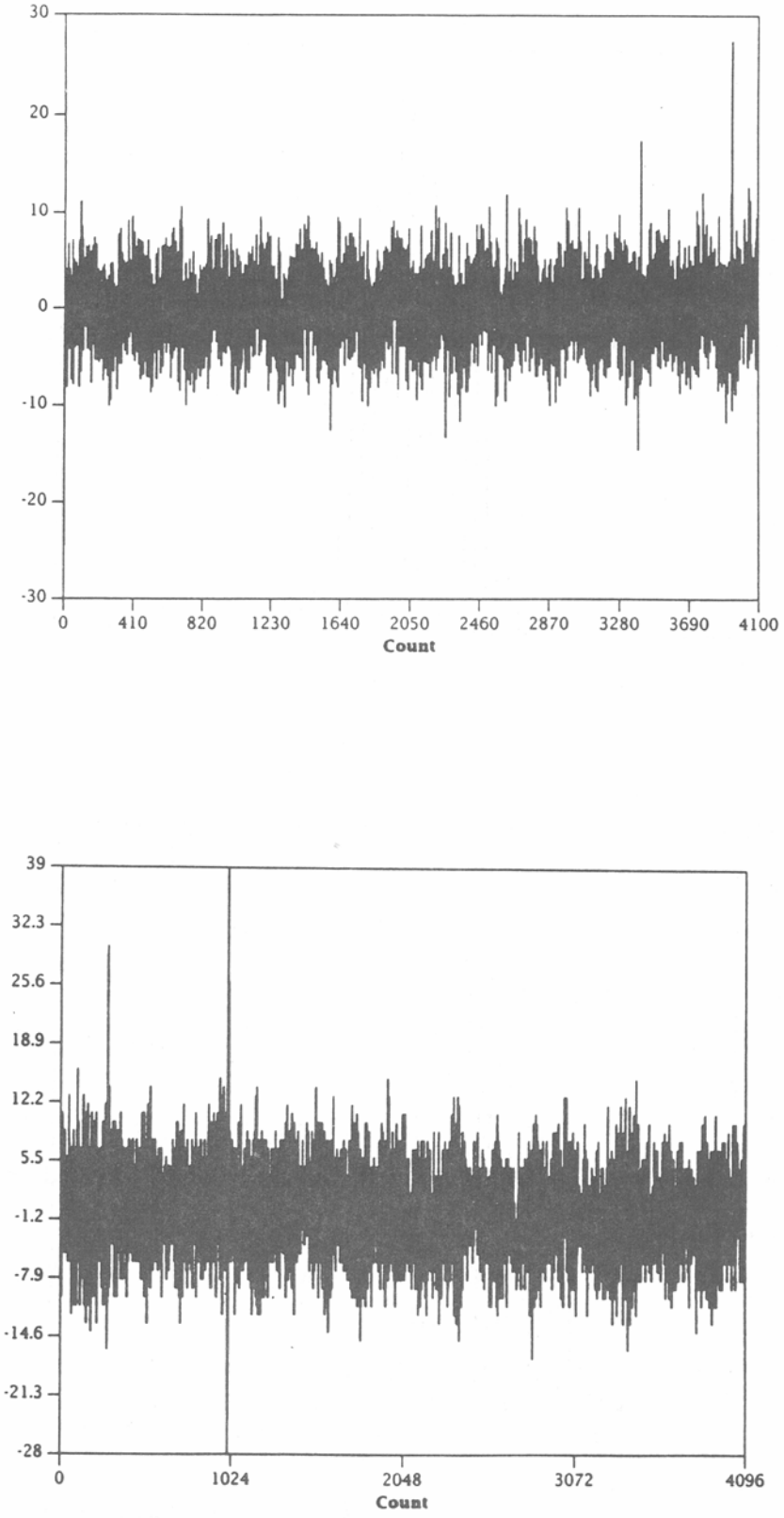

Figure 47. Comparison of (a) simulated and (b) measured (case study 5) I-channel data.

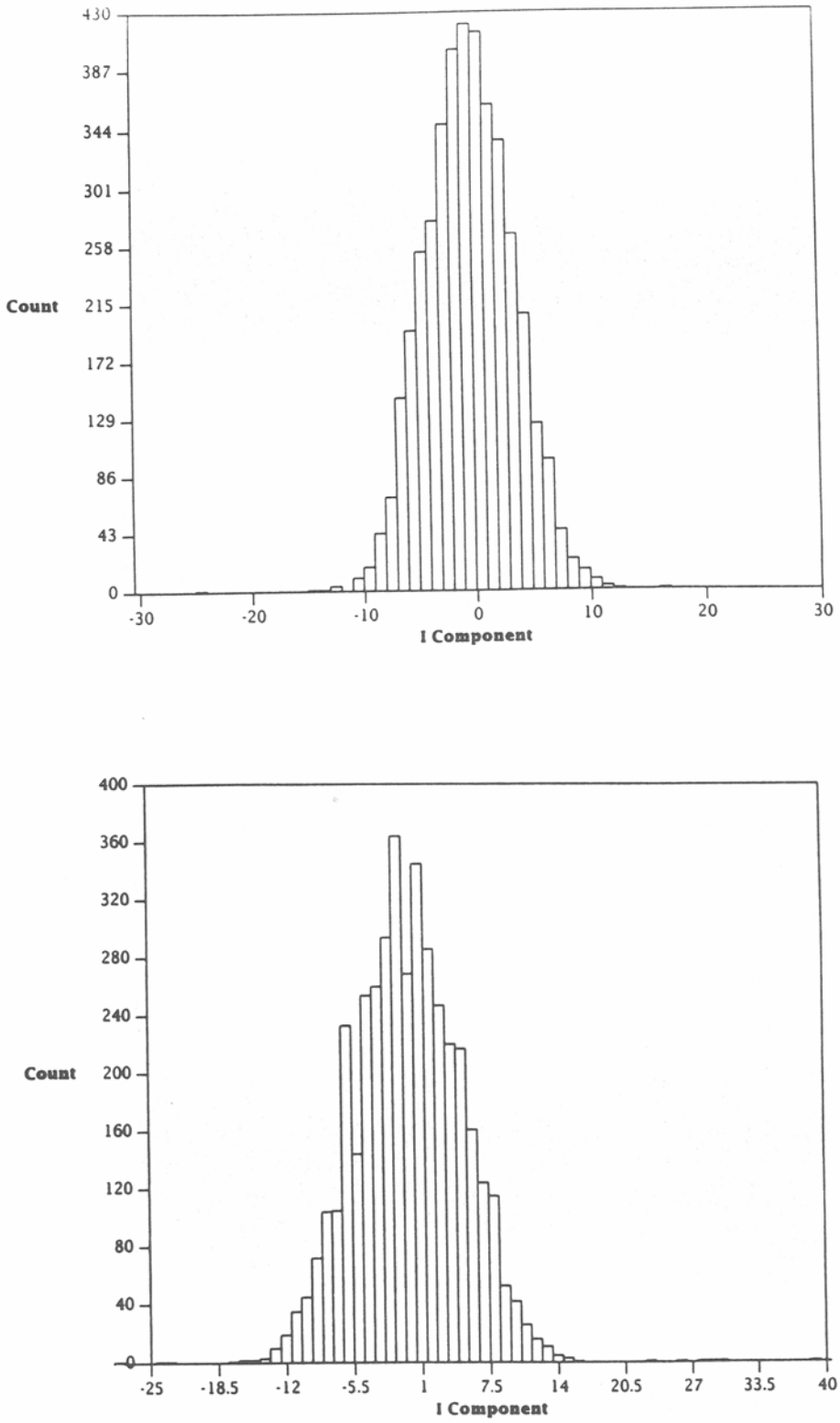

Figure 48. Comparison of (a) simulated and (b) measured (case study 5) probability density functions of the I-channel data.

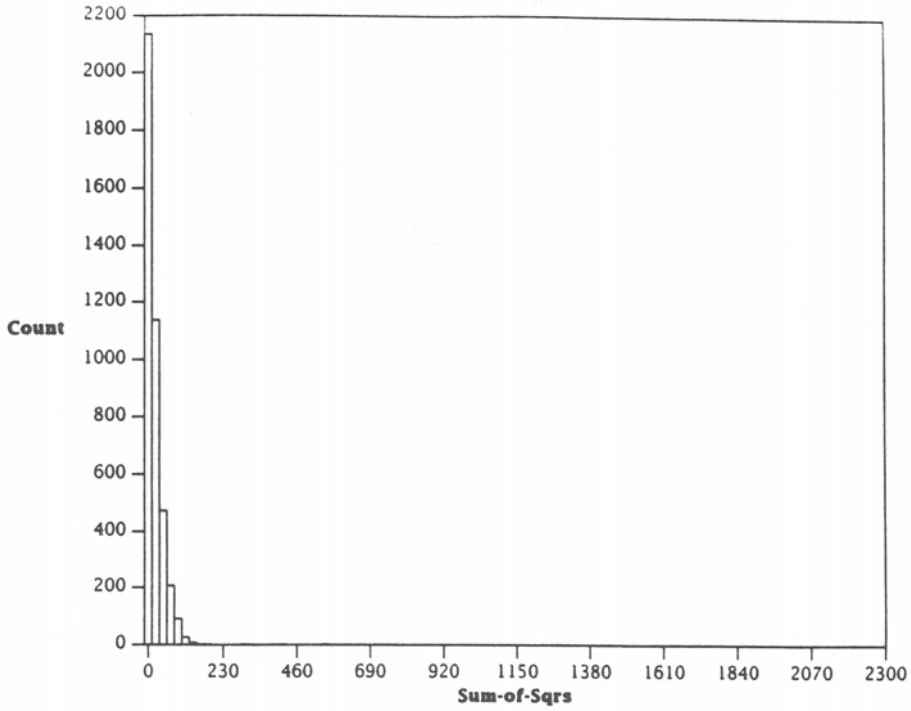

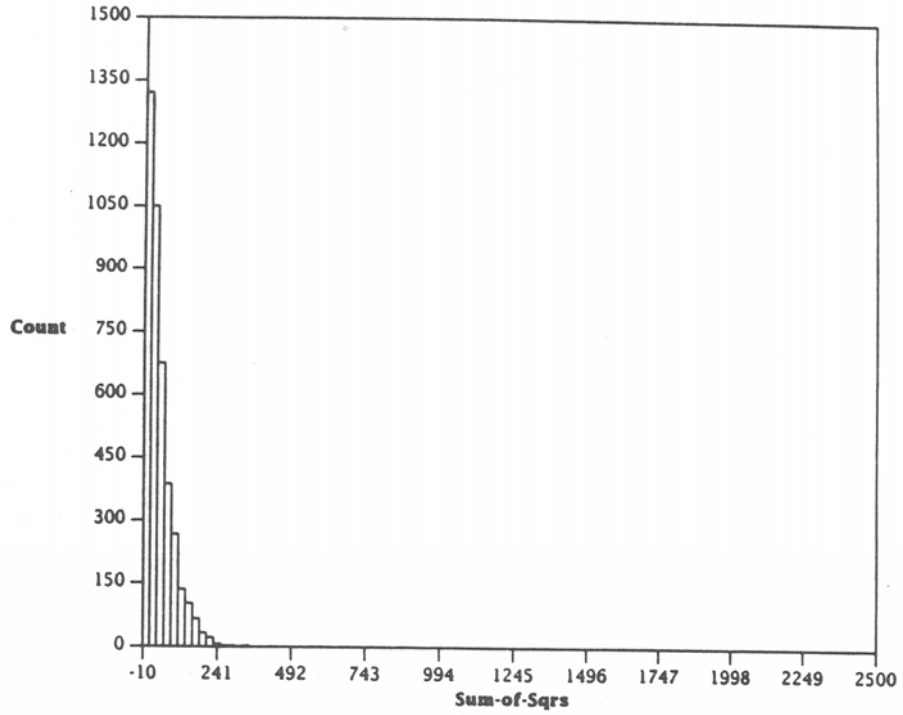

Figure 49. Comparison of (a) simulated and (b) measured (case study 5) probability density functions of the power envelope in the time domain.

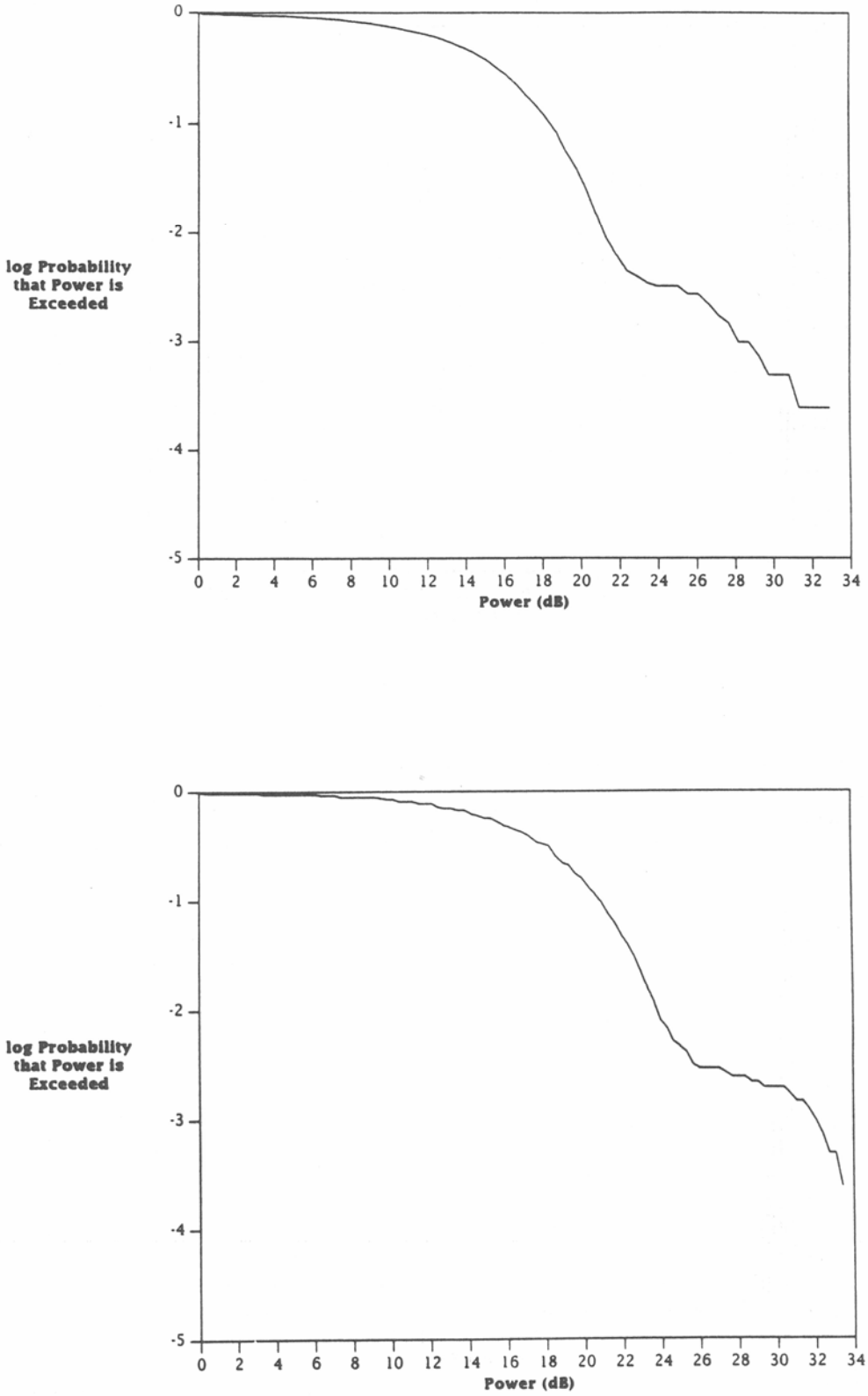

Figure 50. Comparison of (a) simulated and (b) measured (case study 5) cumulative distribution functions of the power envelope in the time domain.

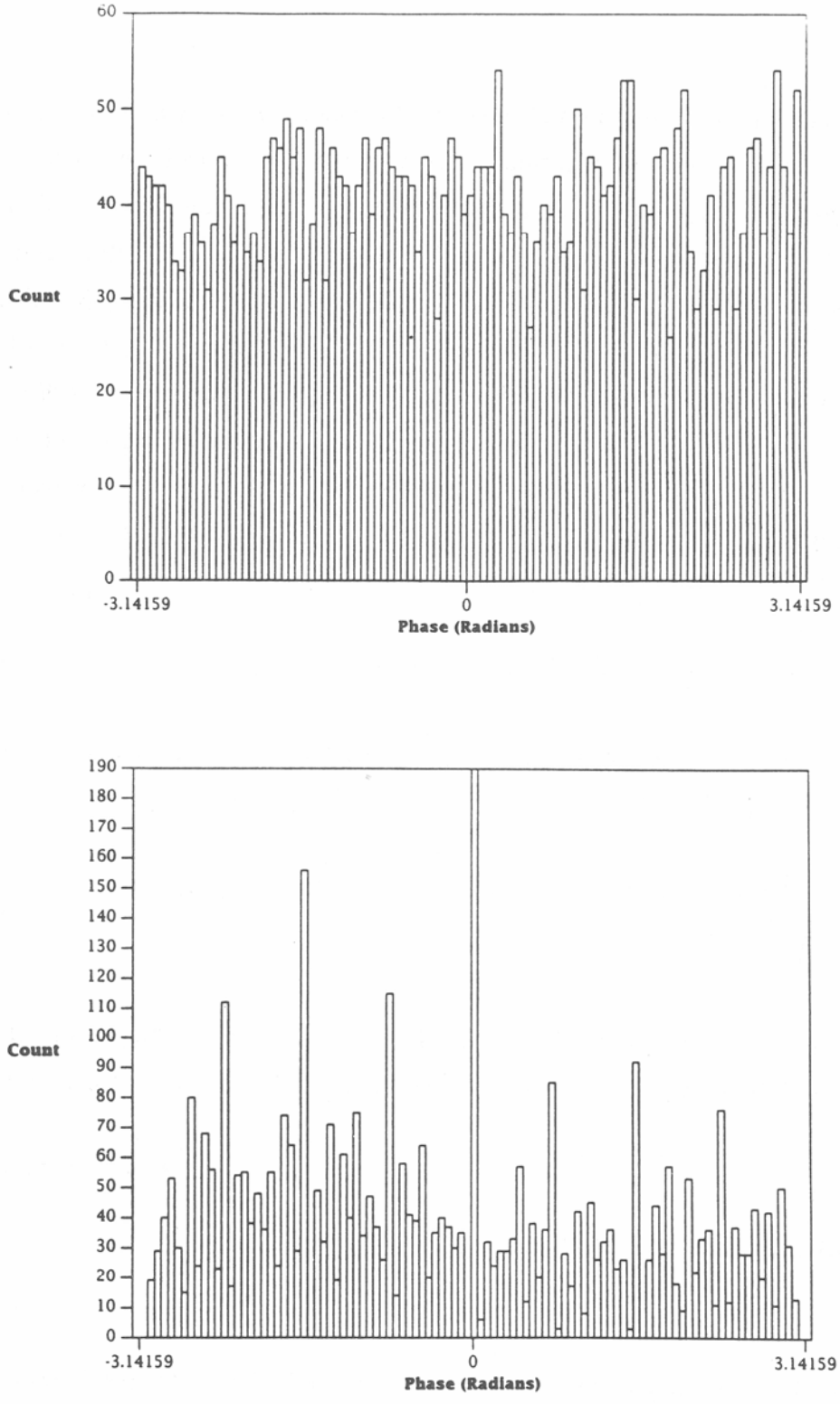

Figure 51. Comparison of (a) simulated and (b) measured (case study 5) probability density functions of the phase in the time domain.

The level crossing distributions of the voltage envelope are shown in Figure 52, and again resemble those of previous case studies, except for the long tails in the distributions.

The power spectra, power cdf's in the frequency domain, and phase pdf's in the frequency domain are shown in Figures 53, 54, and 55, respectively. These quantities resemble those of previous cases, except for the difference of approximately 20 dB in the noise floor of the power spectra between the portions of the band which are inside and outside the bandpass of the filters in the HF receiver. As pointed out above, this difference can be attributed to the presence of a filtered, broadband process (filtered impulses).

It is of interest to compute the relative power of the Gaussian, narrowband, and impulsive components of the noise/interference. Since the power is $I^2 + Q^2$, the average power in the Gaussian component is

$$P_G = \frac{1}{T}\int_0^T \left[g_I^2(t) + g_Q^2(t)\right]dt = \sigma_I^2 + \sigma_Q^2 \qquad \textbf{(26)}$$

where σ_I and σ_Q are the standard deviations of g_I and g_Q, respectively. The power in the narrowband component is

$$\begin{aligned} P_{NB} &= \frac{1}{T}\int_0^T \left\{\left[\sum_i A_i \cos\left(\Delta\omega_i t + \varphi_i\right)\right]^2 + \left[\sum_i A_i \sin\left(\Delta\omega_i t + \varphi_i\right)\right]^2\right\}dt \\ &= \sum_i A_i^2 \end{aligned} \qquad \textbf{(27)}$$

where the integral over the cross-terms in (27) vanishes due to the orthogonality of sines and cosines of different frequencies. The average power of the impulsive component is

$$\begin{aligned} P_{IMP} &= \frac{1}{T}\int_0^T \left\{\left[\sum_j B_j \frac{\sin 2\pi B\left(t - t_j\right)}{t - t_j}\cos\omega_0 t_j\right]^2 + \left[\sum_j B_j \frac{\sin 2\pi B\left(t - t_j\right)}{t - t_j}\sin\omega_0 t_j\right]^2\right\}dt \\ &\approx \frac{\pi B}{T}\sum_j B_j^2 \int_{-\infty}^{\infty} \frac{\sin^2 \pi x}{(\pi x)^2 dx} = \frac{\pi B}{T}\sum_j B_j^2 \end{aligned} \qquad \textbf{(28)}$$

where the cross-terms in (28) which arise from the products of two distinct impulses are assumed to approximately vanish, and where the integral from 0 to T has been approximated by the integral from $-\infty$ to $+\infty$.

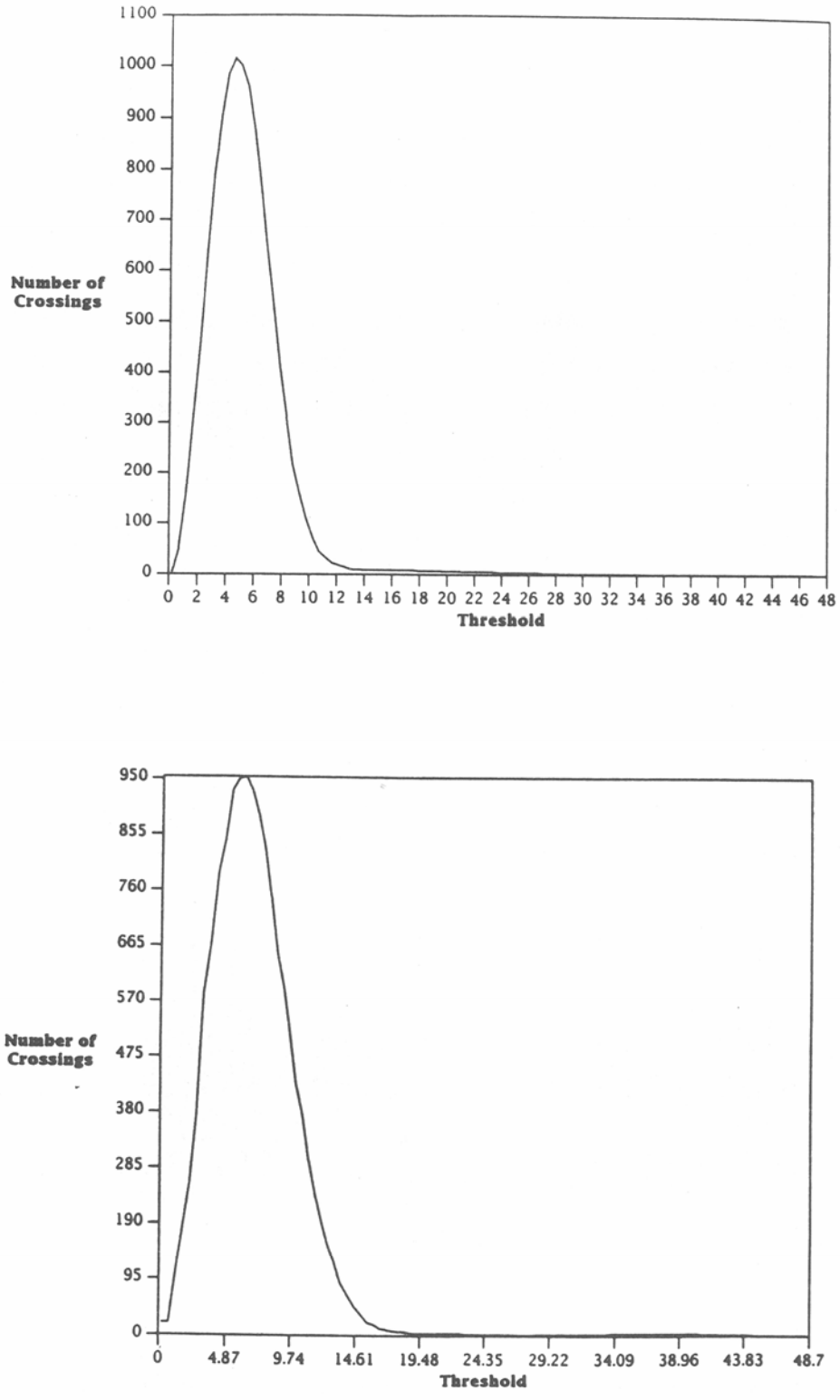

Figure 52. Comparison of (a) simulated and (b) measured (case study 5) level crossing distributions of the voltage envelope.

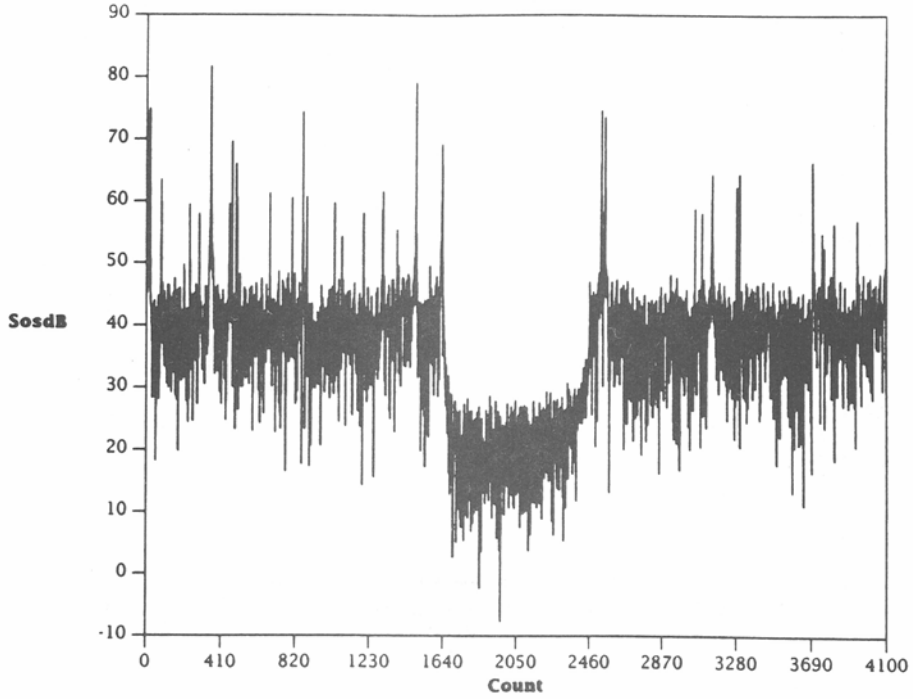

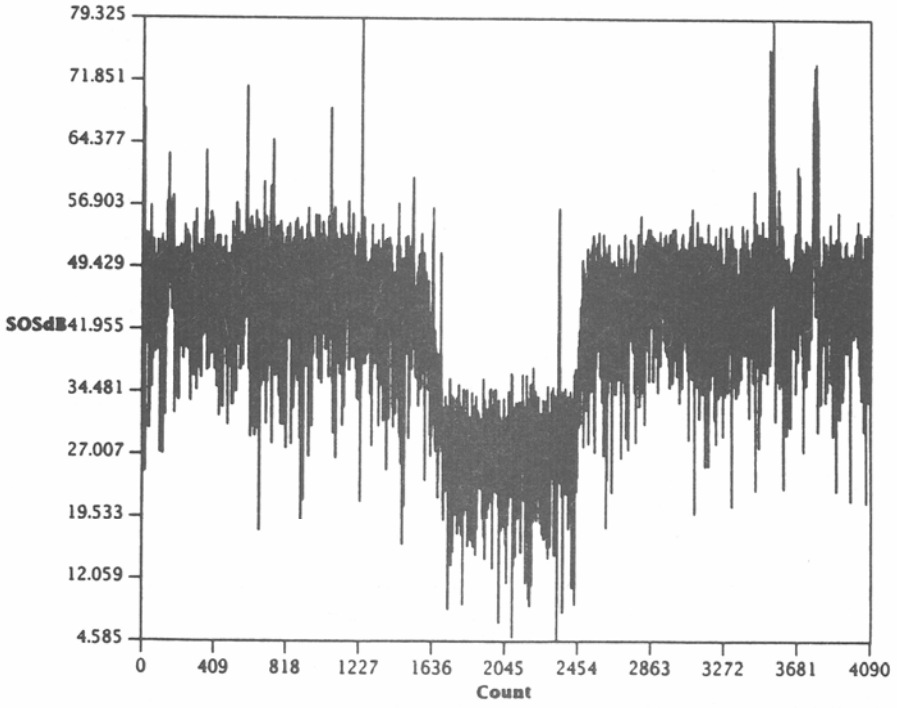

Figure 53. Comparison of (a) simulated and (b) measured (case study 5) power spectra.

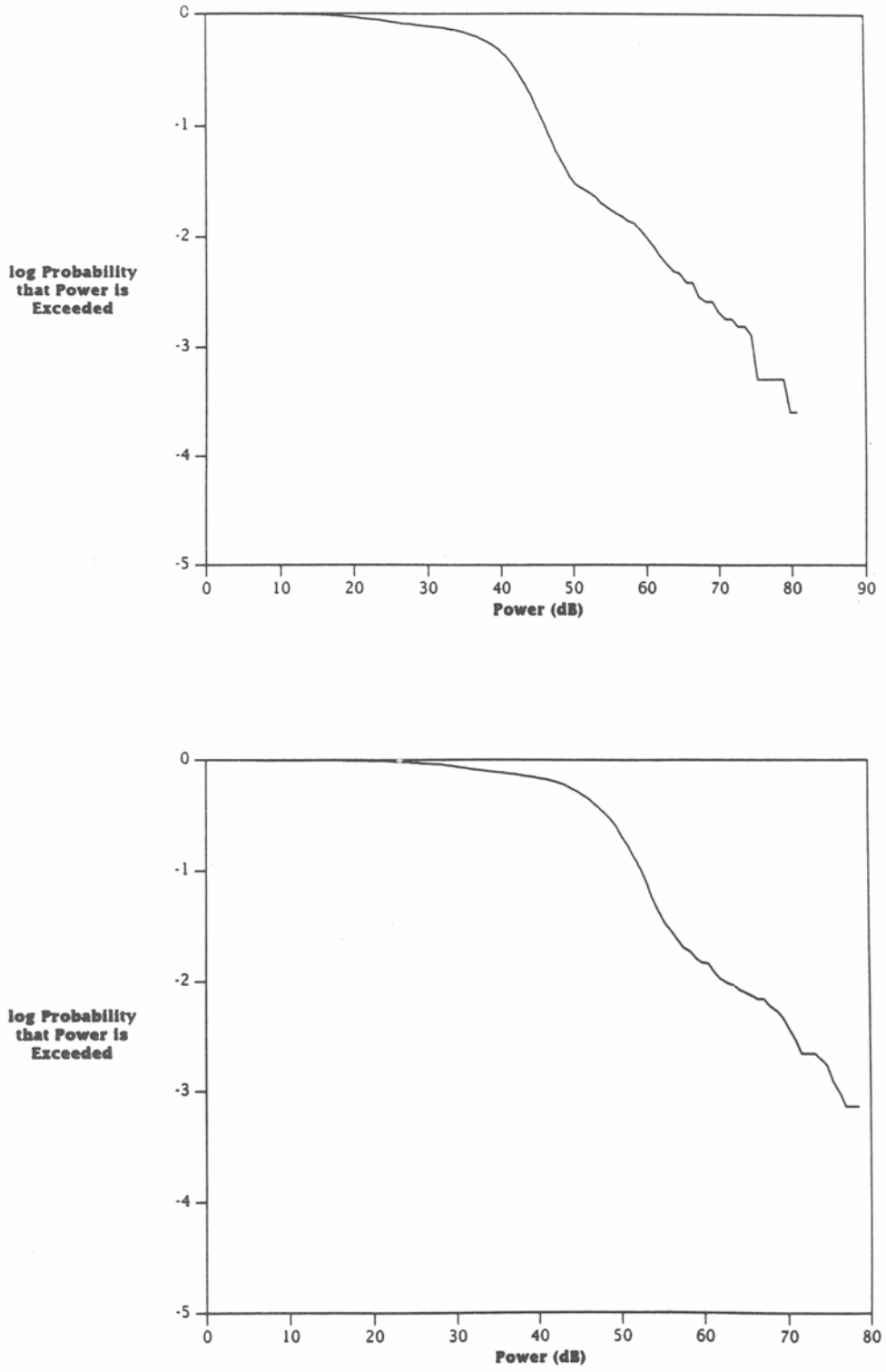

Figure 54. Comparison of (a) simulated and (b) measured (case study 5) cumulative distribution functions of the power envelope in the frequency domain.

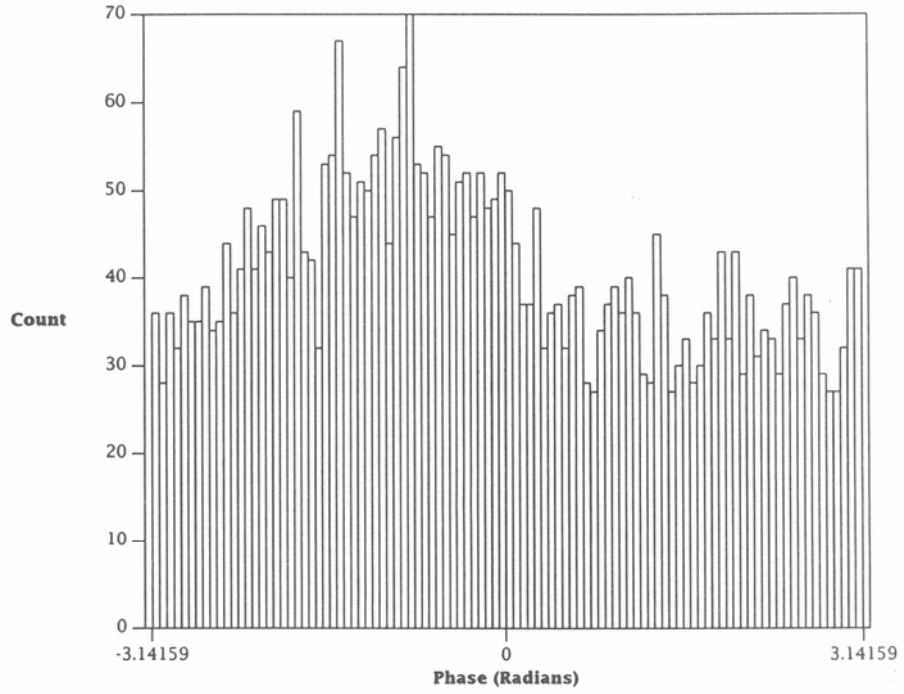

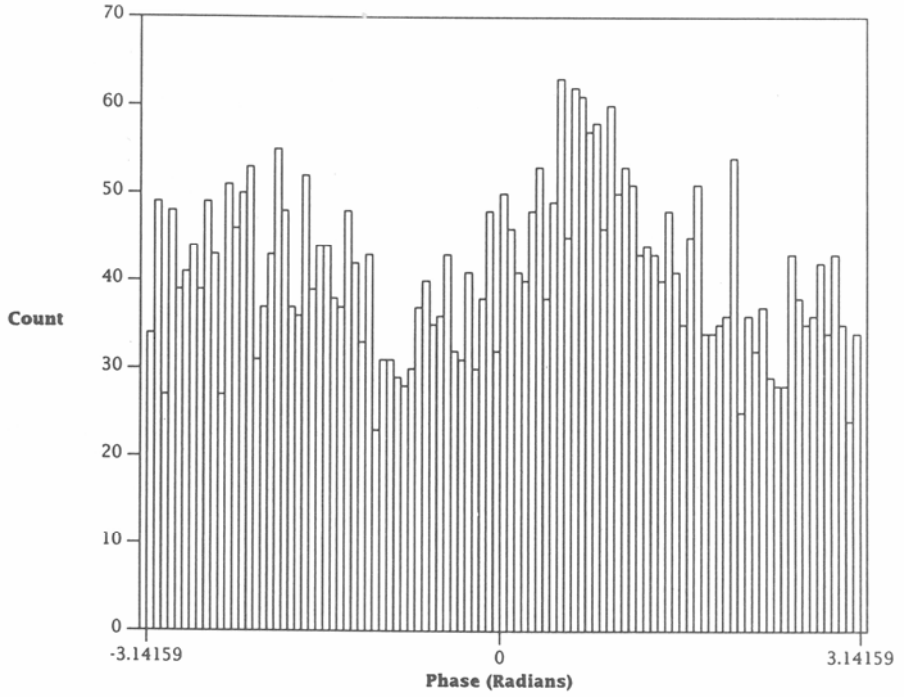

Figure 55. Comparison of (a) simulated and (b) measured (case study 5) probability density functions of the phase in the frequency domain.

In the simulation of noise/interference containing impulsive noise, $\sigma_I = \sigma_Q = 0.12$, $\sum A_i^2 = 28.13$, $\sum B_j^2 = 1.26 \times 10^{-9}$, $B = 2\pi \times 400$ kHz, and $T = 4$ ms. Substituting these values into (26)-(28), one finds that $P_G = 0.0288$, $P_{NB} = 28.13$, and $P_{IMP} = 2.52$. Thus, relative to the Gaussian noise power, the narrowband power is approximately 30 dB and the impulsive power is approximately 19 dB.